analytical chemistry

Article

pubs.acs.org/ac

Three Dimensional Microfluidic Cell Arrays for *ex Vivo* Drug Screening with Mimicked Vascular Flow

Zeynep Dereli-Korkut,[†] H. Dogus Akaydin,[‡] A. H. Rezwanuddin Ahmed,[†] Xuejun Jiang,[§] and Sihong Wang*,[†]

[†]Department of Biomedical Engineering, The City College of the City University of New York, 160 Convent Ave. Steinman Hall T-434, New York, New York 10031, United States

[‡]Department of Mechanical Engineering, Stanford University, Stanford, California 94305, United States

[§]Cell Biology Program, Memorial Sloan-Kettering Cancer Center, New York, New York 10065, United States

Supporting Information

ABSTRACT: Currently, there are no reliable *ex vivo* models that predict anticancer drug responses in human tumors accurately. A comprehensive method of mimicking a 3D microenvironment to study effects of anticancer drugs on specific cancer types is essential. Here, we report the development of a three-dimensional microfluidic cell array (3D μFCA), which reconstructs a 3D tumor microenvironment with cancer cells and microvascular endothelial cells. To mimic the *in vivo* spatial relationship between microvessels and nonendothelial cells embedded in extracellular matrix, three polydimethylsiloxane (PDMS) layers were built into this array. The multilayer property of the device enabled the imitation of the drug delivery in a microtissue array with simulated blood circulation. This 3D μFCA system may provide better predictions of drug responses and identification of a suitable treatment for a specific patient if biopsy samples are used. To the pharmaceutical industry, the scaling-up of our 3D μFCA system may offer a novel high throughput screening tool.

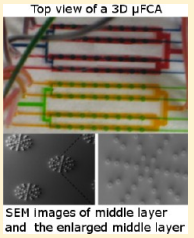

The *in vivo* microenvironment of mammalian cells possesses some common characteristics such as continuous nutrient supply and waste removal, maintenance of an appropriate temperature, short distance between cells and microvessels, cell−cell communication, minimal surrounding stress, and the ratio of cell volume to the extracellular fluid volume greater than one.[1,2] However, current *in vitro* cell culture techniques used in clinical and pharmaceutical drug screening or discovery neither provide these conditions nor simulate the three-dimensional (3D) *in vivo* microenvironment of mammalian cells simultaneously. Although the static 3D cell culture mimics *in vivo* complexity at some levels, main limitations of these culture systems include fast nutrient and O_2 depletion as well as accumulation of metabolites and waste products due to lack of a circulatory mechanism. On the other hand, animal models often provide good results of drug pharmacokinetics but seldom yield reliable outcomes of drug efficacy in human beings.[3] In the cases of anticancer drug development and clinical screening of patient-specific anticancer drugs, lack of accurate 3D *in vitro* cell/tissue models becomes a bottleneck.

The process of tumor progression is influenced by the communication between the tumor cells and the surrounding cells. Therefore, mimicking the microenvironment of tumor cells is essential to study tumor growth and regression.[4,5] Angiogenesis and metastasis are dependent on the tumor microenvironment. The continuity of cancer growth relies on continuous angiogenesis and tumor cell invasion into other organs via blood vessels.[6,7] The conventional 2D cell culture environment causes cancer cells to adopt unnaturally spreading morphology, while cancer cells in 3D culture embrace rounded and clustered morphology similar to tumors *in vivo*.[4,8] Different drug sensitivities were observed for cells grown as a 2D monolayer compared with the same cells grown in 3D culture configurations.[9,10] The growth rate of tumor cells in the 3D environment reflects *in vivo* tumor growth better than that in the 2D environment[5.] Static 3D cell culture techniques lack the engineered microvessels necessary to closely mimic the *in vivo* 3D microenvironment.

Miniaturization of a conventional cell culture system with microfluidic technologies provides an opportunity to model a three-dimensional physiological or pathological environment. A wide range of conditions (e.g., multiple drugs) can be screened simultaneously with high yield on such a platform. Using reverse transfection and a robotic spotter, the first cell microarray for 2D cell culture was developed by the Sabatini group.[11,12] When it is used for drug screening and drug action mechanism discovery, this type of cell microarray generates an enormous volume of data from one compound screening at one condition due to the lack of microfluidic systems. To overcome this limitation, several versions of microfluidic cell arrays for 2D monolayer cell culture were developed with[13,14] or without[15−18] microvalves. Their potential applications were demonstrated broadly from stem cell culture[18] and differentiation[13] to dynamic gene expression profiling.[14] However,

Received: November 12, 2013
Accepted: February 25, 2014

   dx.doi.org/10.1021/ac403899j | *Anal. Chem.* XXXX, XXX, XXX−XXX

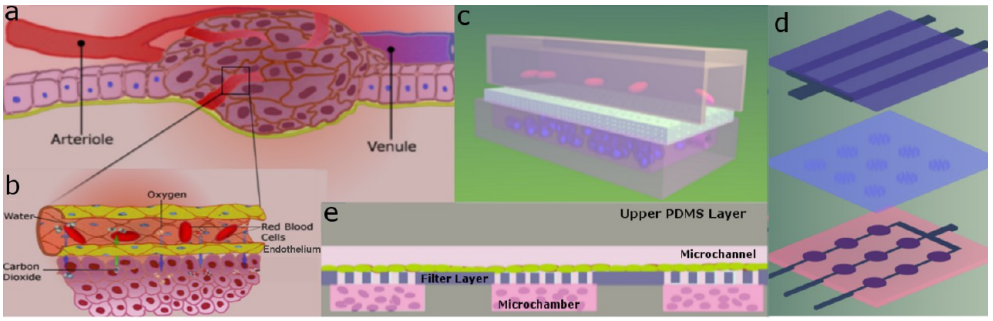

Figure 1. Schematic drawings of tumor microenvironment and 3D microfluidic cell array (μFCA). (a) Tumor microenvironment including cancer cells, surrounding stromal cells, venules, and arterioles; (b) nutrient and gas transport between microvessels and tumor cells; (c) engineering 3D microenvironment by a layered structure; (d) schematics of each layer of 3D μFCA; and (e) cross-section view of 3D μFCA. The bottom layer has microchambers with cancer cells embedded in hydrogel. The middle layer is a permeable membrane with clustered pores. The upper layer has microchannels with seeded endothelial cells to simulate blood microvessels.

these microfluidic cell arrays could not accommodate three-dimensional cell cultures, which are essential to mimic an *in vivo* microenvironment.

Recognizing the inherent laminar flow generated in microfluidic channels, researchers have been able to culture cells encapsulated in 3D matrix on one side of a microchannel and allow fluid flow on the other side of the channel.[19] However, the device with side-by-side 3D culture and flow in the same microchannel without the array architecture is not readily amendable for high throughput screening assays. Additionally, 3D cell microarrays without fluidic components have been reported with an array of cell and matrix droplets created by a robotic spotter and cultured on a glass slide.[20,21] Without a simulated microcirculation system, these 3D cell microarrays were unlikely able to closely mimic the *in vivo* 3D microenvironment for high throughput drug screening.

In this study, we developed a 3D microfluidic cell array (μFCA) consisting of three PDMS (polydimethylsiloxane) layers to model *in vivo* microenvironment. The parametric study using computational fluid dynamics simulation was performed on the designed geometric variables based on three-dimensional microfluidic cell array (3D μFCA) to study their effects on the profiles of flow and nutrient delivery. The three-layer design enabled 3D hydrogel encapsulation cell culture in an array of microchambers adjacent to multiple separated microchannels seeded with endothelial cells to serve as bioartificial blood vessels. Using this technology, multiple stimuli including clinical and potential anticancer drugs were applied on a 3D microtumor array on a single chip to measure dynamic responses of apoptotic activities. This study has thus established a potentially high throughput screening method that combines microfluidic technology and 3D cell culture techniques to monitor the dynamic responses of potential or clinical anticancer drugs in a simulated 3D microenvironment with microcirculation.

■ EXPERIMENTAL SECTION

3D microfluidic cell array (μFCA) consists of: (i) microchannels to simulate blood microvessels, (ii) microchambers in a different layer for 3D cell culturing in extracellular matrix, and (iii) a membrane with clustered pores at specific locations to guide the diffusion in between the layers of microchannels and microchambers. Thus, nutrient supply and waste removal for cells encapsulated 3D matrix are maintained via diffusion from and to a continuous flow of fresh medium in the microchannels. Soft lithography was used to fabricate each layer with polydimethylsiloxane (PDMS). Briefly, silicon etching was employed in master making of three layers. A set of food color dyes was used to verify the diffusion from the top to bottom layers through clustered pores in the middle layer on a 3D μFCA. The detailed methods of the device manufacture and testing are explained in Supporting Information I (ac403899j_si_001.pdf).

A computational fluid dynamics (CFD) simulation was performed in FLUENT (Ansys, Inc.) to investigate the theoretical similarity of dynamic cell culture conditions maintained by the 3D μFCA microchambers to interstitial flow conditions *in vivo*. The studied geometry was a cross section of one unit on the device along the thickness with three parts, one microchamber, one group of pores, and one microchannel. Detailed procedures of computational modeling are explained in Supporting Information II (ac403899j_si_002.pdf).

Three types of cells were used in this study, human ductal breast epithelial tumor cell line (T47D), human non-small cell lung cancer cell line (PC9), and adult human dermal blood microvascular endothelial cells (HMVEC). Cancer cells were encapsulated using PuraMatrix hydrogel in its viscous liquid form and flowed into the bottom microchambers of a 3D μFCA, followed by cell growth medium in the top channels to trigger the gel polymerization in the bottom. No visible cell density variations were observed in the different microchambers when the cell density of the cell−gel mixture was the same. Cell culture was maintained by continuous flow in the top channel using a syringe pump. Short and long-term cell viability in our μFCA was evaluated using calcein AM, a fluorescence live cell dye. Structured coculture between PC9 and HMVECs in a 3D μFCA was achieved by seeding HMVECs in the top microchannels following the seeding of PC9 cells in hydrogel in the bottom microchambers. In the case of coculture, cancer cells were dyed with DiI, a red fluorescence long term cell tracker. Four apoptotic inducers (i.e., Tarceva, staurosporine, TNF-α, and colchicines) were applied to compare the caspase-3 activities of PC9 cell cultures in conventional culture dishes with that in the 3D microenvironment generated in a 3D μFCA. Caspase-3 activities were measured using DEVD-Nucview 488, a green fluorescence probe to detect activated caspase-3. Detailed materials and methods related to biological experiments in this study are explained in Supporting Information I (ac403899j_si_001.pdf).

A fully automated epi-fluorescence microscope equipped with an objective moving in the *z* direction and a stage

dx.doi.org/10.1021/ac403899j | *Anal. Chem.* XXXX, XXX, XXX−XXX

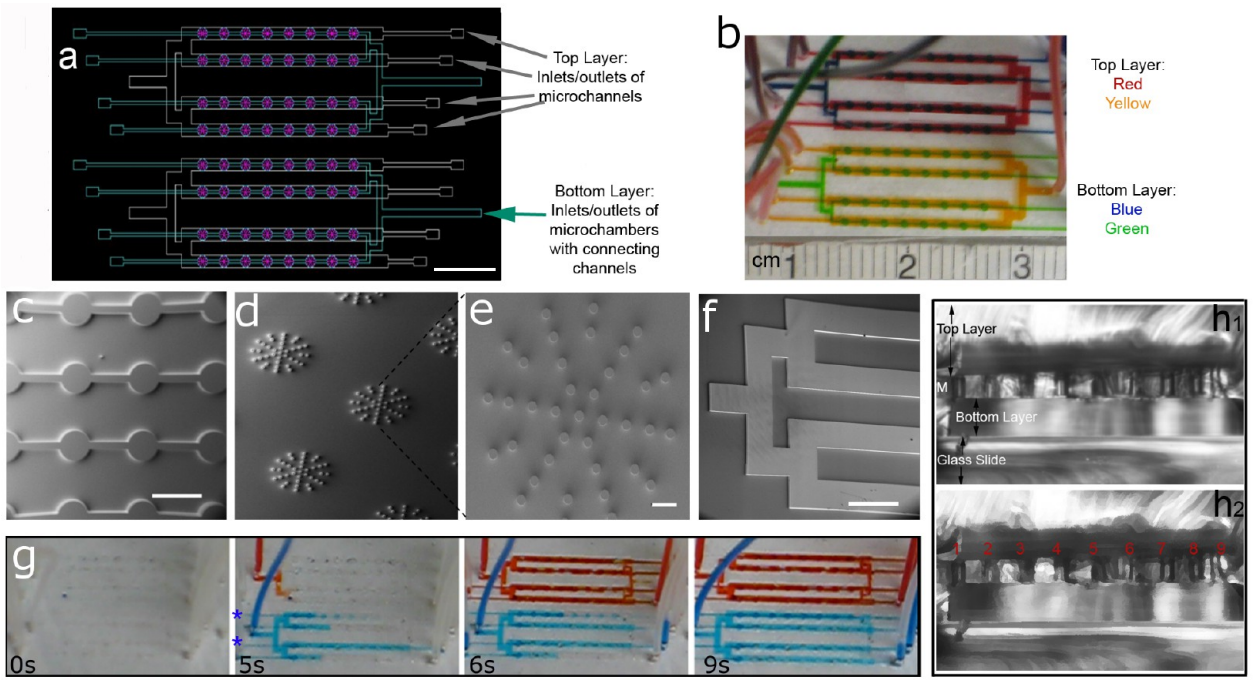

Figure 2. Design and fabrication of 3D microfluidic cell arrays. (a) AutoCAD device mask drawing of merged layers, scale bar is 2 mm; (b) top view of a 3D μFCA with a solid/nonpermeable PDMS middle layer, features dyed with blue and green food colors are in the bottom while red and yellow channels are in the top layer; SEM images of silicon etched masters of (c) bottom (scale bar is 1 mm), (d) middle, and (f) upper layers (scale bar is 1 mm); (e) SEM image of the enlarged middle layer; master scale bar is 100 μm; (g) frames of a video showing diffusion of food dyes from top to bottom layers through the middle filter layer in 5 s (two blue stars [*] point to two channels on the bottom which become blue due to dye diffusion from the top); side-view of one unit of 3D microfluidic cell arrays (μFCA) captured under a 5× phase contrast objective showing (h_1) three PDMS layers bonded on a glass slide ("M" indicates the middle PDMS layer with clustered pores) and (h_2) numbered pores in the middle layer in a dry brush processed image using Photoshop.

controller of temperature and CO_2 were used to take wide-field *z*-stack fluorescence images for 3D cell culture. Time-lapse of 3D images were taken during the drug treatment. Quantitative fluorescence image analysis was performed after deconvolution of 3D *z*-stack images. The detailed methods of 3D image capture and analysis are explained in Supporting Information I (ac403899j_si_001.pdf).

RESULTS

The tumor microenvironment with blood vessels illustrated in Figure 1a,b was modeled using a bioengineering approach via a layered microstructure (Figure 1c). In order to be able to scale up for future high throughput drug screening, the array concept was included as illustrated in Figure 1d. Figure 1e is the schematic drawing of a cross-section view of a 3D μFCA with an endothelial cell layer over the filter layer to mimic the physical 3D *in vivo* structure.

Operation of the 3D μFCA. Figure 2a is a merged image of AutoCAD drawings of all three masks for: (i) the top layer with 8 white straight microchannels, (ii) the middle porous layer with 64 groups of micropores represented by purple stars, and (iii) the bottom layer including 64 microchambers in green. In order to show the features in top and bottom layers clearly, different food colors were introduced in a 3D μFCA with a nonpermeable PDMS middle layer. Features dyed with blue and green are in the bottom layer while red and yellow microchannels are on the top (Figure 2b). Scanning electron microscopy (SEM) images of masters of three layers show that the diameter of microchambers is 770 μm (Figure 2c) and the pore size on the middle filter layer (Figure 2d,e) is 40 μm. The large pore size was chosen aiming to hold the endothelial cells atop the tumor mass while permitting the maximum exchange of nutrients and waste products. The vasculature of growing tumors is known to be very porous compared to normal vasculurate.[22] In a 3D μFCA, pores are grouped and positioned so that they are right above the microchambers when the bottom microchamber layer is permanently bonded with the middle PDMS porous layer. The top layer (Figure 2f) is composed of 790 μm wide microchannels. The microchannel width is close to the upper range (>500 μm) of pulmonary vessel's diameter.[23]

One of the main operations in a 3D μFCA is diffusion between different layers of the device. Such diffusive transport is critical for communication among cells in different layers. For this purpose, the diffusion efficiency was tested between layers using a set of food dyes. Figure 2g includes four frames of a video captured during the top-to-bottom-layer diffusion test. When food dyes were introduced through inlets of the top layer with closed inlets and outlets of the bottom layer, food dyes reached to the bottom layer within 5 s (Figure 2g). These results verified that the middle PDMS layer was porous and diffusion from top to the bottom layer occurred in seconds. The clustered pores in the middle layer enabling this guided diffusion between top and bottom layers are displayed in Figure 2h, which shows the cross-section (i.e., side-view) of one unit of a 3D μFCA including three PDMS layers on a glass substrate to visually capture the three-dimensional feature of the device.

Diffusion and Microcirculation Profile Using Computational Fluid Dynamics (CFD) Analysis. Simulation data conclude that vertical diffusion between different layers plus convection flow in the top microchannels is sufficient for

dx.doi.org/10.1021/ac403899j | *Anal. Chem.* XXXX, XXX, XXX−XXX

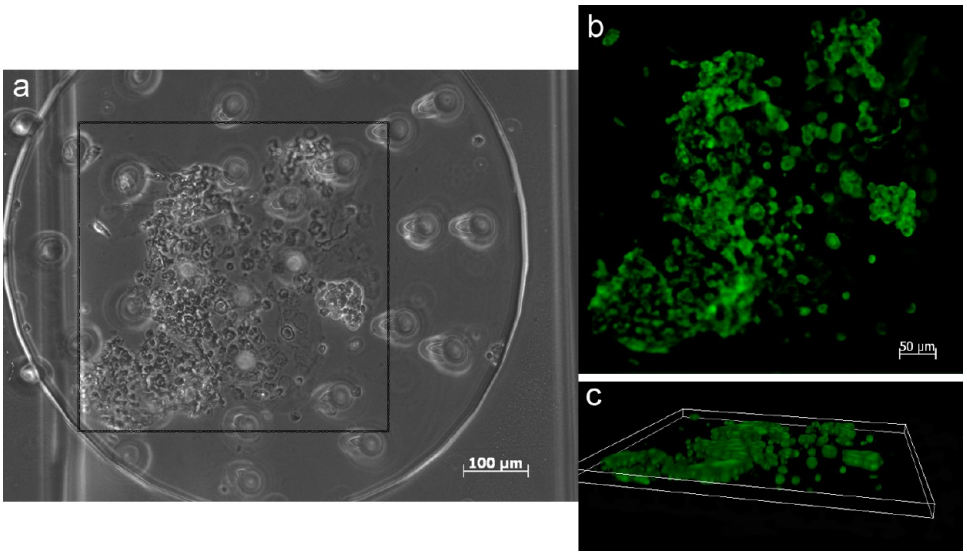

Figure 3. Lung cancer cells with long fluorescence trackers encapsulated in hydrogel and cultured in a chamber of a 3D μFCA for 15 days, (a) phase contrast image, (b) 2D projected image after deconvolution of fluorescence z-stack images, and (c) 3D view of (b), where its dimension is 550 × 500 × 70 μm in x (length from left to right), y (depth), and z (thickness from bottom to top) directions.

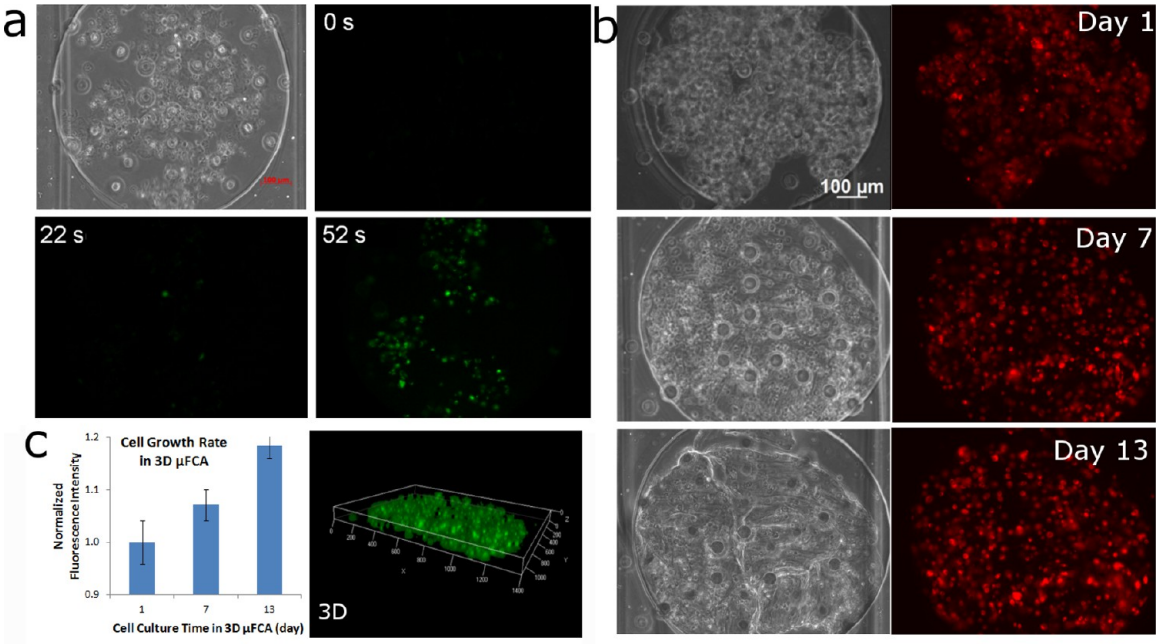

Figure 4. Short and long-term cell viability in the 3D μFCA culture. (a) Short-term cell viability images including a phase contrast picture of breast cancer cells embedded in hydrogel and its time-lapse fluorescence green images at 0, 22, and 52 s after the introduction of calcium Am in the top microchannels. Scale bar is 100 μm. Live cells are fluorescence green; (b) phase contrast and fluorescence red images of long-term culture of lung cancer PC9 cells in 13 days. The increase of red fluorescence intensity confirmed cell growth; (c) cell growth rate (n = 3) and 3D reconstructed image of long-term lung cancer cell culture on day 13 after adding calcein AM to verify long-term viability.

nutrient delivery and waste removal in the 3D μFCA. There is an extremely low advective flow at ~0.1 μm/s in the bottom microchamber without hypoxia. The decrease in O_2 concentrations from the microchannel inlet to bottom right corner of the same microchamber is less than 0.0003%. With 10 to 100 microchambers in a serial connection, there will be no hypoxia in the last microchamber in our current device with the microchamber thickness of 100 μm. However, hypoxia conditions in the late stage of tumors can be mimicked by increasing the thickness of microchambers in the future. Detailed results including a figure of computational modeling are explained in Supporting Information II (ac403899j_si_002.pdf).

Reconstructed 3D Cell Images from *z*-Stack Epi-fluorescence Images via Deconvolution. To evaluate the imaging ability of 3D live cell culture in a 3D μFCA using an epi-fluorescence microscope equipped with an objective moving in the z-direction, lung cancer cells were dyed with a green fluorescent long-term cell tracker before hydrogel encapsulation and then cultured in the microchambers of the bottom layer of the device for two weeks with initial cell seeding density of 10 million/mL. Using 1 μm per z-slice over

dx.doi.org/10.1021/ac403899j | Anal. Chem. XXXX, XXX, XXX−XXX

cell aggregates of 70 to 80 μm in depth, deconvolution results are shown in Figure 3, which includes a projected image (Figure 3b) and the reconstructed 3D image (Figure 3c) of cancer cell aggregates cultured in a chamber of the 3D μFCA on day 15.

High Cell Culture Viability in the 3D μFCA. Short and long-term cell viability in a 3D μFCA is essential for accurate drug screening. For a one week culture in a 3D μFCA, viability of breast cancer T47D cells with initial cell seeding density of 10 million/mL on Day 7 is shown in Figure 4a, which includes a 10× phase contrast image of T47D cells encapsulated in PuraMatrix and fluorescence images of cells at 0, 22, and 52 s after the calcein AM introduction in top microchannels. Vertical diffusion of calcein AM from top microchannels to bottom microchambers was indicated by the fluorescence green signal observed as early as 22 s. At 52 s, most of the cells were fluorescence green demonstrating high cell viability in the 3D μFCA. In the long term viability test, PC9 cells were stained with DiI red fluorescence cell tracker before hydrogel encapsulation and seeding in a 3D μFCA with initial cell seeding density of 60 million/mL. Figure 4b shows phase contrast and fluorescence images of DiI stained PC9 cells on Day 1, 7, and 13. The gradual increase of red fluorescence signal indicates the cell growth in the device (Figure 4c). High cell viability assessed by calcein AM on Day 13 for the long-term culture in the device is also shown in Figure 4c, which is a three-dimensional reconstructed green fluorescence image deconvoluted from a stack of PC9 cell images captured after calcein AM staining.

Microtumor Cell Aggregates with Mimicked Microvessels in a 3D μFCA. Structured coculture between DiI prestained cancer cells and microvascular endothelial cells in a 3D μFCA is shown by phase contrast and corresponding fluorescence images in Figure 5. A fluorescence red cancer cell aggregate is presented in a microchamber in bottom-focused images (Figure 5b) while monolayer endothelial cells indicated by arrows are clearly pictured in the top-focused phase contrast image (Figure 5c). Thus, a microchannel with endothelial cells serves as a biomimicked microvessel, and the middle PDMS membrane with clustered micropores ensures the diffusion-controlled transport of metabolites and the communication between cancer cells and their microenvironment. Anticancer reagents have to diffuse through the mimicked microvessels and then reach tumor mass, which is a scenario much closer to *in vivo* drug delivery.

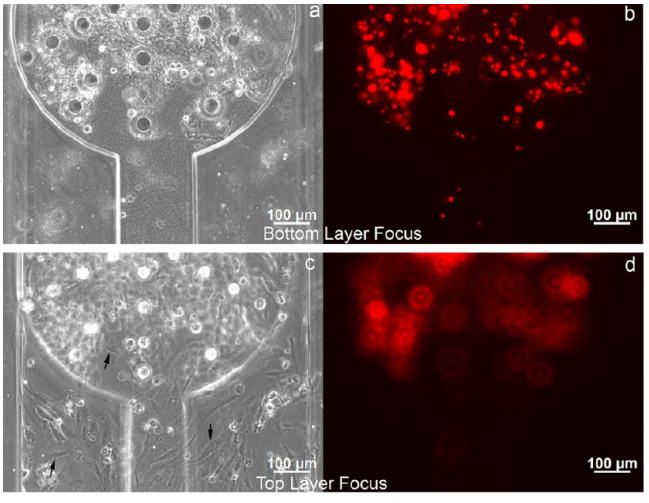

Figure 5. Coculture between PC9 lung cancer cells in the bottom round microchambers and endothelial cells in the top microchannels in a 3D μFCA. (a, c) Phase contrast and (b, d) their corresponding fluorescence images of DiI prestained PC9 cell aggregates in hydrogel and human microvascular endothelial cells (HMVEC, no staining) seeded in the microchannels of the top layer. Images at different focus planes are displayed to show both cell types. Arrows point to some endothelial cells.

Profiles of Caspase-3 Activity in Different Culture Configurations. We demonstrated the potential of the 3D μFCA for dynamic anticancer drug screening by monitoring apoptotic response to clinical or potential anticancer drugs. Figure 6a includes representative time-lapse fluorescence images showing caspase-3 activities in PC9 cells in conventional static 2D cultures treated with Tarceva (Tar), staurosporine (Sta), TNF-α with cycloheximide (TNF-α/CHX), colchicine (Col), and caspase-3 inhibitors (Cas 3 In) at 0, 3, and 17 h of stimulation. Results of quantitative fluorescence image analysis in Figure 6b show that there is a rapid increase of active caspase-3 in PC9 cells treated by three drugs (Tarceva, staurosporine, and TNF-α with cycloheximide) in the early stage of stimulation, followed by a graduated elevation of activated caspase-3 along the stimulation. However, responses to colchicine are much slower and lower than the other three drugs until 12 h after drug stimulations. At 17 h, the staurosporine treatment led to the highest caspase-3 activity followed by TNF-α/CHX, colchicine, and Tarceva, in descending order.

The dynamics of drug responses in conventional static 3D PC9 encapsulation cultures (Figure 6c) or PC9/microvascular endothelial cell cocultures (Figure 6d) are very different from that of 2D cultures. Comparison of 2D (Figure 6b) and 3D (Figure 6c) PC9 alone cultures shows that caspase-3 activities were lower in the 3D encapsulation culture. Interestingly, both the static 3D encapsulation cultures (Figure 6c,d) had higher drug responses in the early stage of stimulation rather than the late stage. This phenomenon is vividly demonstrated in Figure 6f,g, which are representative 3D reconstructed images of PC9 cultures and PC9/endothelium cocultures in peptide hydrogel stimulated by Tarceva, respectively.

In the 3D μFCA culture condition, endothelial and PC9 cells are structurally cocultured in different layers but communicate with each other through clustered micropores in the middle PDMS membrane in between. In drug treated samples, caspase-3 activities increase slowly but steadily until 6 h when they reach the highest level (Figure 6e). This is followed by a slight decrease afterward. Figure 6h is representative 3D reconstructed images of caspase-3 activities of cocultures in a 3D μFCA under the stimulation of Tarceva. Comparison of Figure 6d,e demonstrated that cells in structured cocultures using mimicked *in vivo* microenvironment have slower and lower maximum drug responses than the static 3D random coculture where cells experience drugs directly. The maximum drug response in structured cocultures in a 3D μFCA was reached at 6 h vs 3 h in the unstructured static 3D coculture in tissue culture plates. We speculate that the endothelium formed in the top microchannels worked as a drug barrier layer to delay the drug delivery.

DISCUSSION

In this study, we demonstrated that high viabilities of short (Figure 4a) and long-term (Figure 4b) cancer 3D cultures

dx.doi.org/10.1021/ac403899j | Anal. Chem. XXXX, XXX, XXX−XXX

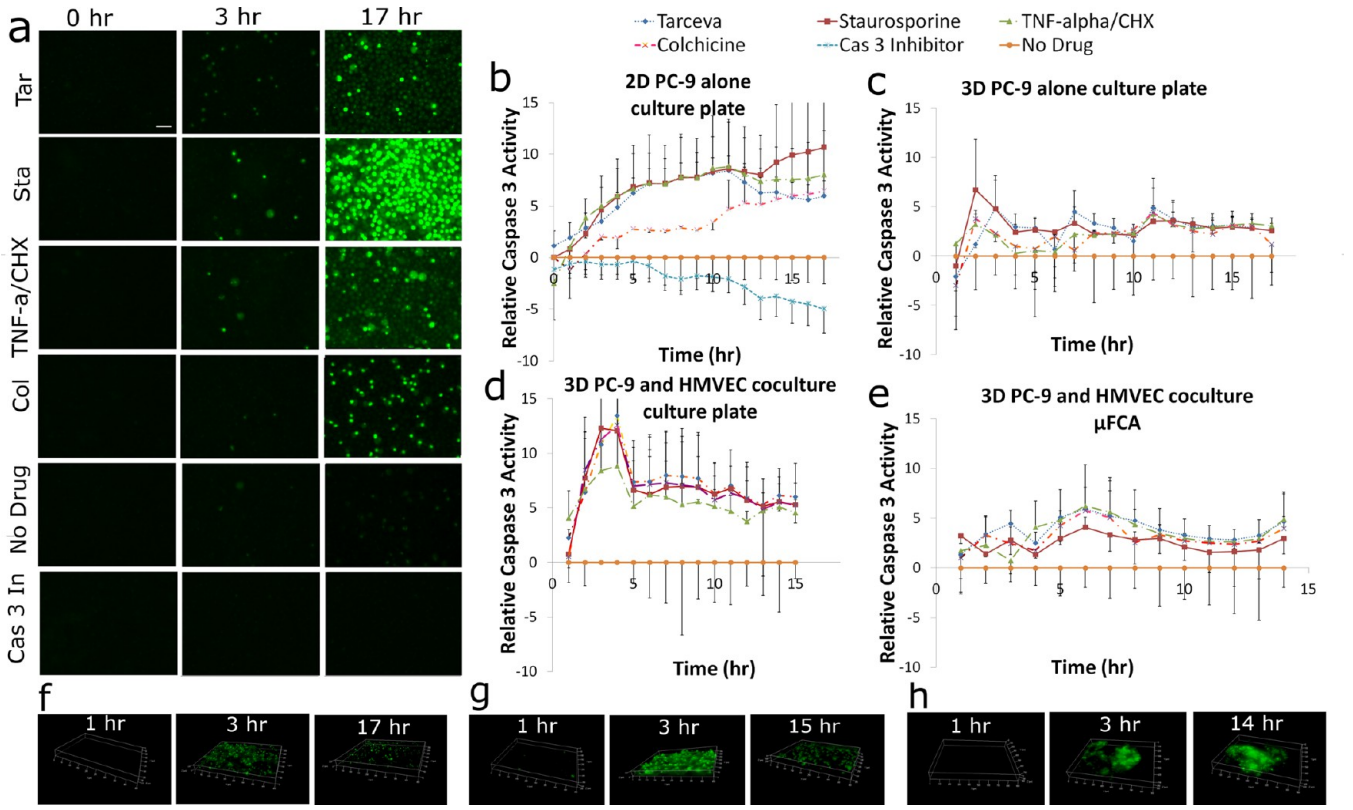

Figure 6. Dynamic caspase-3 activities of anticancer compounds in different culture conditions. (a) Fluorescence images of drug treated PC9 cells for 17 h in 2D conventional culture; quantitative image analysis of drug treated (b) PC9 cells in 2D conventional cell culture (n = 4), (c) PC9 cells in conventional 3D cultures (n = 4), (d) coculture of PC-9/HMVEC in 3D conventional cell culture (n = 4), and (e) structural coculture of PC-9/HMVEC in 3D μFCA, where relative caspase-3 activity = $\log_2(FI/FI_{no\text{-}drug})$, in which FI means fluorescence intensity (n = 4); 3D reconstructed fluorescence images of Tarceva treated PC9 cells in (f) 3D conventional culture, (g) 3D conventional coculture of PC9/HMVEC, and (h) structural coculture of PC9/HMVEC in 3D μFCA.

could be achieved in our 3D μFCA using different initial cell seeding densities (i.e., 10 and 60 million/mL). Tumor tissues have a wide range of cellularity from 10% to 90% depending on cancer types and stages.[24−27] The seeding density of 60 million/mL in the bottom microchambers of our current 3D μFCA gives about 90% cellularity. For a purpose of drug screening, different cell seeding densities in a 3D μFCA can be used to achieve the simulation of different stages of cancer. Additionally, using this 3D μFCA, lung cancer cells grown as microtumor aggregates in microchambers were structurally cocultured with endothelial cells in microchannels mimicking microvessels under continuous flow to simulate blood circulation (Figure 5). The efficacy of anticancer drugs in terms of their effects on apoptosis of cancer cells was evaluated in the 3D μFCA coculture system (Figure 6e,h). In addition, computational fluid dynamics (CFD) simulation showed that the 3D μFCA created a microenvironment for cells where the mechanical stresses are extremely low with about 0.1 μm/s flow velocity in cell microchambers and the nutrients and waste products were efficiently transported via diffusion and extremely low convection (Supporting Information II, Figure 1 (ac403899j_si_002.pdf)).

Conventional cell culture techniques for drug screening are dominated by 2D cell culture. Recently introduced 3D cell culture techniques showed the significant impacts of the 3D tumor structure on cellular microenvironments on cell growth, cell morphology, gene profile, and drug sensitivities.[28,29] Previous microfluidic devices designed potentially for high throughput drug screening were focused on 2D monolayer cell culture.[11,13,14,16−18] However, it is essential to mimic *in vivo* conditions to obtain realistic results of biological processes.[30,31] In the previous systems, cancer cells were seeded directly inside microchannels or microchambers without 3D extracellular matrix, so cells are in direct contact with fluid flow.[14,16,17,32] Such direct flow applies shear stresses on cells which are not present *in vivo* except for endothelial cells and duct epithelial cells (e.g., alveolar and kidney epithelial cells). A simplified kidney chip and lung chip used mechanical stresses provided by microfluidic systems in the design.[33,34] However, diffusion is the main transport mechanism *in vivo* between tissues and microvessels or capillaries. The 3D μFCA realized the diffusion process for the transportation of nutrients, metabolic waste products, and other molecules by the three layer structure. The flow velocity of 0.1 μm/s in microchambers of a 3D μFCA obtained by the CFD simulation is similar to the *in vivo* interstitial flow, which is 0.1−1 μm/s.[35]

On the other hand, employing the laminar flow property of microfluidic channels and micropillars as barriers, a microfluidic device was managed to have cells embedded in 3D matrix at the center of a channel and medium flow at both sides of the same channel.[36,37] Lateral diffusion in the same channel maintained 3D cell culture. However, this microfluidic system would allow low throughput measurements. Using our 3D μFCA, real time measurements of multiple drug responses in different types of cancer cells cultured in a 3D microenvironment with simulated blood vessels could be recorded in single experiments on single

dx.doi.org/10.1021/ac403899j | *Anal. Chem.* XXXX, XXX, XXX−XXX

chips (Figure 6). Furthermore, by changing the bonding orientation between the top microchannel layer and the bottom microchamber layer from currently parallel to orthogonal alignments, the second generation of 3D μFCA will be a powerful tool for high throughput drug screening with closely mimicked 3D microenvironment in an array format. Different strategies including adding microvalves are under investigation to prevent drug leakage between microchambers.

In this study, direct visualization and quantitative analysis of apoptotic responses via caspase-3 activities in PC9 cells cocultured with HMVECs in 3D μFCA and exposed to four anticancer drugs were a confirmation of the system versatility for potential high throughput drug screening (Figure 6). Dynamic caspase-3 activities in PC9 cells showed that cancer cells had different drug responses in different culture platforms, such as static 2D or 3D culture, static 3D coculture, and structured 3D cocultured in the 3D μFCA with simulated blood vessels. In the conventional static culture conditions, PC9 cells had greater drug responses in 2D monolayer culture than that of cancer cells embedded in 3D matrix (Figure 6b,c). Studies from other researchers also showed different drug responses of cancer cells depending on the cell culture environment.[4,38] Interestingly, static 3D coculture between PC9 cells and HMVECs brought the low drug responses back to a similar level as the 2D monolayer culture (Figure 6b,d). This result indicates that drug responses are dependent on the 3D microenvironment and cells themselves. Therefore, it is essential to construct an *in vitro* system to mimic an *in vivo* tumor microenvironment including proper cell types in order to obtain reliable anticancer drug responses in drug screening.

The drug response results of the current static 3D environment are not reliable due to the lack of a circulation mechanism to remove the waste products and toxic byproducts. This was confirmed by the different dynamic (e.g., slower and reduced) drug responses in the structured coculture of lung cancer cells with microvascular endothelial cells in our 3D μFCA compared with the static random coculture (Figure 6d,e). We speculate that the attenuated and delayed drug responses from PC9 and cocultures in our 3D μFCA are caused by a HMVEC monolayer formed in the top layer of the device, shown in Figure 5c. Several experimental optimization and measurements related to the top endothelial layer need to be performed to achieve microvessels as close to *in vivo* as possible. For example, the seeding density of HMVECs and length of the HMVEC culture before drug testing need to be optimized by matching diffusive permeability of top endothelial layer to *in vivo* data. The diffusive permeability can be measured using fluorescence labeled dextran molecules.[39] In addition, tight junctions between HMVECs can be verified by VE-cadherin immunostaining.[39] Once the top endothelial layer is fully optimized, analog phenomena to tumor angiogenesis and metastasis can be studied in our 3D microfluidic cell arrays.

Although an attempt to construct a layered microfluidic device was made by stacking a microchannel layer on top of a two-microchamber layer with an opaque polyester membrane in the middle,[40] this design is not suitable for scaling up to an array structure for high throughput drug screening due to the leakage possibility across neighboring microchambers/channels caused by the property of nonselective perfusion directions of the polyester membrane, which is permeable vertically and laterally. The nontransparent semipermeable membrane makes fast imaging of 3D cell culture in different layers extremely difficult without confocal microscopy, which is not commonly used in high throughput drug screening due to its slow scanning speed. Our 3D μFCA is a pure PDMS device to overcome limitations mentioned above.

Our novel 3D microfluidic cell arrays established an *in vitro* microtumor/tissue array to mimic an *in vivo* 3D microenvironment with simulated blood vessels. Furthermore, integration of techniques of microvalve and cell seeding without tubing into the current design will open the possibility for high-throughput analysis and clinical translation. Evidence shows that cancer cell behavior, including progression and drug resistance, is affected by its host microenvironment consisting of direct contact with tumor stroma and soluble factors secreted from tumor stroma.[41,42] Therefore, other types of stromal cells besides endothelial cells (e.g., fibroblasts) in tumor tissues will be incorporated in the next generation of our 3D microfluidic cell arrays (μFCA). On the other hand, thin (about 250 μm in thickness)[43,44] and thick (1−2 mm in thickness)[45−47] tissue slides have been cultured successfully in nonarray-format microfluidic devices with perfusion for hours to a couple of days depending on tissue types. This encourages us to further modify our 3D μFCA to accommodate tissue samples (e.g., biopsy tissues) directly instead of performing 3D tissue reconstruction in our next model. It will lead to the clinical applications of using our 3D μFCA to search for more effective and personalized medicine in cancer treatments.

In summary, our 3D microfluidic cell array (3D μFCA) provides a novel technology to mimic an *in vivo* 3D microenvironment using an *ex vivo* platform that is readily amendable to screen anticancer drugs for a personalized therapy or to scale up for high throughput drug screening in the pharmaceutical industry.

■ ASSOCIATED CONTENT

Ⓢ Supporting Information

Additional information as noted in the text. This material is available free of charge via the Internet at http://pubs.acs.org.

■ AUTHOR INFORMATION

Corresponding Author

*E-mail: shwang@ccny.cuny.edu.

Notes

The authors declare no competing financial interest.

■ ACKNOWLEDGMENTS

This study was supported by NIH/NCI 1U54CA137788 (CCNY-MSKCC Partnership) and partially funded by NSF CBET-1055608 (NSF CAREER award to S.W.). This work was performed in part at the Cornell NanoScale Facility, a member of the National Nanotechnology Infrastructure Network, which is supported by the National Science Foundation (Grant ECS-0335765).

■ REFERENCES

(1) Walker, G. M.; Zeringue, H. C.; Beebe, D. J. *Lab Chip* **2004**, *4*, 91−97.
(2) Vaupel, P. *Semin. Radiat. Oncol.* **2004**, *14*, 198−206.
(3) Nyga, A.; Cheema, U.; Loizidou, M. *J. Cell Commun. Signaling* **2011**, *5*, 239−248.
(4) Gurski, L. A.; Jha, A. K.; Zhang, C.; Jia, X.; Farach-Carson, M. C. *Biomaterials* **2009**, *30*, 6076−6085.
(5) Chignola, R.; Schenetti, A.; Andrighetto, G.; Chiesa, E.; Foroni, R.; Sartoris, S.; Tridente, G.; Liberati, D. *Cell Proliferation* **2000**, *33*, 219−229.

(6) Kim, Y.; Stolarska, M. A.; Othmer, H. G. *Prog. Biophys. Mol. Biol.* **2011**, *106*, 353−379.
(7) Joyce, J. A.; Pollard, J. W. *Nat. Rev. Cancer* **2009**, *9*, 239−252.
(8) Feder-Mengus, C.; Ghosh, S.; Reschner, A.; Martin, I.; Spagnoli, G. C. *Trends Mol. Med.* **2008**, *14*, 333−340.
(9) Serebriiskii, I.; Castello-Cros, R.; Lamb, A.; Golemis, E. A.; Cukierman, E. *Matrix Biol.* **2008**, *27*, 573−585.
(10) Doillon, C. J.; Gagnon, E.; Paradis, R.; Koutsilieris, M. *Anticancer Res.* **2004**, *24*, 2169−2177.
(11) Ziauddin, J.; Sabatini, D. M. *Nature* **2001**, *411*, 107−110.
(12) Bailey, S. N.; Ali, S. M.; Carpenter, A. E.; Higgins, C. O.; Sabatini, D. M. *Nat. Methods* **2006**, *3*, 117−122.
(13) Gomez-Sjoberg, R.; Leyrat, A. A.; Pirone, D. M.; Chen, C. S.; Quake, S. R. *Anal. Chem.* **2007**, *79*, 8557−8563.
(14) King, K. R.; Wang, S.; Irimia, D.; Jayaraman, A.; Toner, M.; Yarmush, M. L. *Lab Chip* **2007**, *7*, 77−85.
(15) Hung, P. J.; Lee, P. J.; Sabounchi, P.; Lin, R.; Lee, L. P. *Biotechnol. Bioeng.* **2004**, *89*, 1−8.
(16) Lee, P. J.; Hung, P. J.; Rao, V. M.; Lee, L. P. *Biotechnol. Bioeng.* **2006**, *94*, 5−14.
(17) Thompson, D. M.; King, K. R.; et al. *Anal. Chem.* **2007**, *76*, 4098−4103.
(18) Kim, L.; Vahey, M. D.; Lee, H. Y.; Voldman, J. *Lab Chip* **2006**, *6*, 394−406.
(19) Aref, A. R.; Huang, R. Y.; Yu, W.; Chua, K. N.; Sun, W.; Tu, T. Y.; Bai, J.; Sim, W. J.; Zervantonakis, I. K.; Thiery, J. P.; Kamm, R. D. *Integr. Biol. (Cambridge, U. K.)* **2013**, *5*, 381−389.
(20) Flaim, C. J.; Chien, S.; Bhatia, S. N. *Nat. Methods* **2005**, *2*, 119−125.
(21) Albrecht, D. R.; Underhill, G. H.; Wassermann, T. B.; Sah, R. L.; Bhatia, S. N. *Nat. Methods* **2006**, *3*, 369−375.
(22) Yuan, F.; Dellian, M.; Fukumura, D.; Leunig, M.; Berk, D. A.; Torchilin, V. P.; Jain, R. K. *Cancer Res.* **1995**, *55*, 3752−3756.
(23) Cavallotti, C.; D'Andrea, V.; Cavallotti, C.; Cameroni, M. *Geriatr. Gerontol. Int.* **2005**, *5*, 286−292.
(24) Fedorov, L.; Gol'tsova, T. A.; Rozanov Iu, M. *Eksp. Onkol.* **1988**, *10* (63), 66−69.
(25) Goransson, H.; Edlund, K.; Rydaker, M.; Rasmussen, M.; Winquist, J.; Ekman, S.; Bergqvist, M.; Thomas, A.; Lambe, M.; Rosenquist, R.; Holmberg, L.; Micke, P.; Botling, J.; Isaksson, A. *PLoS One* **2009**, *4*, No. e6057.
(26) Rajan, R.; Poniecka, A.; Smith, T. L.; Yang, Y.; Frye, D.; Pusztai, L.; Fiterman, D. J.; Gal-Gombos, E.; Whitman, G.; Rouzier, R.; Green, M.; Kuerer, H.; Buzdar, A. U.; Hortobagyi, G. N.; Symmans, W. F. *Cancer* **2004**, *100*, 1365−1373.
(27) Tanaka, K.; Yamamoto, D.; Yamada, M.; Okugawa, H. *Breast* **2004**, *13*, 334−340.
(28) Haycock, J. W. *Methods Mol. Biol.* **2011**, *695*, 1−15.
(29) Gurski, L. A.; Petrelli, N. J.; Jia, X.; Farach-Carson, M. C. *Oncol. Issues* **2010**, *31*, 20−25.
(30) Freeman, A. E.; Hoffman, R. M. *Proc. Natl. Acad. Sci. U. S. A.* **1986**, *83*, 2694−2698.
(31) Vescio, R. A.; Redfern, C. H.; Nelson, T. J.; Ugoretz, S.; Stern, P. H.; Hoffman, R. M. *Proc. Natl. Acad. Sci. U. S. A.* **1987**, *84*, 5029−5033.
(32) Ye, N.; Qin, J.; Shi, W.; Liu, X.; Lin, B. *Lab Chip* **2007**, *7*, 1696−1704.
(33) Nakao, Y.; Kimura, H.; Sakai, Y.; Fujii, T. *Biomicrofluidics* **2011**, *5*, 22212.
(34) Huh, D.; Matthews, B. D.; Mammoto, A.; Montoya-Zavala, M.; Hsin, H. Y.; Ingber, D. E. *Science* **2010**, *328*, 1662−1668.
(35) Tarbell, J. M.; Shi, Z. D. *Biomech. Model. Mechanobiol.* **2012**, *12*, 111−121.
(36) Choudhury, D.; Mo, X.; Iliescu, C.; Tan, L. L.; Tong, W. H.; Yu, H. *Biomicrofluidics* **2011**, *5*, 22203.
(37) Toh, Y. C.; Zhang, C.; Zhang, J.; Khong, Y. M.; Chang, S.; Samper, V. D.; van Noort, D.; Hutmacher, D. W.; Yu, H. *Lab Chip* **2007**, *7*, 302−309.
(38) Weaver, V. M.; Lelievre, S.; Lakins, J. N.; Chrenek, M. A.; Jones, J. C.; Giancotti, F.; Werb, Z.; Bissell, M. J. *Cancer Cell* **2002**, *2*, 205−216.
(39) Zervantonakis, I. K.; Hughes-Alford, S. K.; Charest, J. L.; Condeelis, J. S.; Gertler, F. B.; Kamm, R. D. *Proc. Natl. Acad. Sci. U. S. A.* **2012**, *109*, 13515−13520.
(40) Song, J. W.; Cavnar, S. P.; Walker, A. C.; Luker, K. E.; Gupta, M.; Tung, Y. C.; Luker, G. D.; Takayama, S. *PLoS One* **2009**, *4*, No. e5756.
(41) Muerkoster, S.; Wegehenkel, K.; Arlt, A.; Witt, M.; Sipos, B.; Kruse, M. L.; Sebens, T.; Kloppel, G.; Kalthoff, H.; Folsch, U. R.; Schafer, H. *Cancer Res.* **2004**, *64*, 1331−1337.
(42) Wang, W.; Li, Q.; Yamada, T.; Matsumoto, K.; Matsumoto, I.; Oda, M.; Watanabe, G.; Kayano, Y.; Nishioka, Y.; Sone, S.; Yano, S. *Clin. Cancer Res.* **2009**, *15*, 6630−6638.
(43) van Midwoud, P. M.; Merema, M. T.; Verpoorte, E.; Groothuis, G. M. *Lab Chip* **2010**, *10*, 2778−2786.
(44) van Midwoud, P. M.; Merema, M. T.; Verweij, N.; Groothuis, G. M.; Verpoorte, E. *Biotechnol. Bioeng.* **2011**, *108*, 1404−1412.
(45) Cheah, L. T.; Dou, Y. H.; Seymour, A. M.; Dyer, C. E.; Haswell, S. J.; Wadhawan, J. D.; Greenman, J. *Lab Chip* **2010**, *10*, 2720−2726.
(46) Hattersley, S. M.; Dyer, C. E.; Greenman, J.; Haswell, S. J. *Lab Chip* **2008**, *8*, 1842−1846.
(47) Hattersley, S. M.; Sylvester, D. C.; Dyer, C. E.; Stafford, N. D.; Haswell, S. J.; Greenman, J. *Ann. Biomed. Eng.* **2012**, *40*, 1277−1288.